Charge Transfer Cross Sections for Multiply Charged Slow Ne, Ar, Kr and Xe Ions on Various Gas Targets I. Rare Gas Targets

By

Toshio KUSAKABE*, Hirofumi HANAKI**,
Nobuo NAGAI**, Tadahiko HORIUCHI**,
Ichiro KONOMI** and Masakatsu SAKISAKA**

Abstract

Observed charge transfer cross sections are compiled in an energy region from a few to tens keV for multiply charged Ne, Ar, Kr and Xe ions on rare gas targets, where projectile ions are produced by using an "ion-impact ion source" (IIIS). The values are compared with the results of other research workers.

1. Introduction

During the past ten years, many theoretical and experimental works have been carried out concerning charge transfer collisions between multiply charged slow ions with various atoms and molecules. The reason is that these collisions are fundamental processes in atomic physics. chemistry, radiation physics, astrophysics[1] and fusion researches[2]. Pre- and post-electronic states of both projectile and target, collision energy, interaction range, emitted radiations and electrons, and cross section magnitude are necessary quantities to be studied, but the observations are not easy.

It was in 1978 that we started the project "low energy ion-atom collisions", because we succeeded in extracting multiply charged recoil ions. When rare gas atoms were bombarded with an accelerator beam of heavy ions and the charge spectra of recoil ions were analyzed with the use of a Wien filter, amounts of highly ionized ions having energies of approximately a few eV width were detected[3]. This system was immediately turned to an ion source applicable to ion-atom collisions in a low energy

---

* Department of Nuclear Reactor Engineering, Kinki University, Kowakae, Higashi-osaka.
** Department of Nuclear Engineering.

region. Thereafter, we named this the "ion-impact ion source" (IIIS), and the feature of the revised system has been reported elsewhere[4].

In an earlier stage of our project, the single- and double-electron captures of He^{2+} ions from He, Ne, Ar, Kr, Xe and N_2 had been studied in the energy region of $0.7-4.5$ keV[3,5]. The detection method for charge-transferred ions was rather simple. Fortunately, since we received the 1979—1981 Scientific Research Expenditure of the Ministry of Education, the experimental apparatus and techniques have been remarkably improved. New data have been rapidly accumulated, which are quite important in considering collision mechanism.

Among very many observed results, we present here the charge transfer cross sections for variously stripped Ne, Ar, Kr and Xe ions on rare gas targets. The projectile-target combinations and the collision energies are listed in Table 1. Our cross section values, tabulated and depicted in many figures, are compared with those of other research workers.

Table 1. Combination of projectile-target in charge transfer experiment.

Projectile Ion	Charge q	Collision energy	Target atom
Ne^{q+}	$2\sim 5$	$1.5q-12q$ keV	He
Kr^{q+}	4, 8	$1.5q-12q$ keV	He
Ar^{q+}	$2\sim 7$	11.4 keV (0.286 keV/amu)	He
Kr^{q+}	$2\sim 9$	24 keV (0.286 keV/amu)	He, Ne, Ar, Kr, Xe
Xe^{q+}	$2\sim 11$	37.6 keV* (0.286 keV/amu)	He, Ne, Ar, Kr, Xe

* A few Xe^{2+}-target combinations were measured at about 34.5 keV in energy (0.262 keV/amu) to prevent an electrical breakdown in ion acceleration.

2. Experimental

The experimental arrangement is schematically shown in Fig. 1, which is fundamentally the same as reported elsewhere[4], but is briefly described here.

2.1. Collision system

A beam of molecular nitrogen ions (N_2^+) with 1 MeV in energy, extracted from a Van de Graaff accelerator of Kyoto University, was sharply collimated up to about $0.2mm \times 3mm$ in size and introduced into an ionization chamber with a beam intensity of $0.05-1.5$ μA. In this chamber was constructed the IIIS, which was composed of two parallel plates, a central gas nozzle, a focusing lens and four accelerating electrodes. When gas atoms ejected from the nozzle were bombarded with the nitrogen beam, highly charged recoil ions were produced. By imposing appropriate electric potentials to the plates, lens and electrodes, recoil ions could be drawn out toward the grounded side.
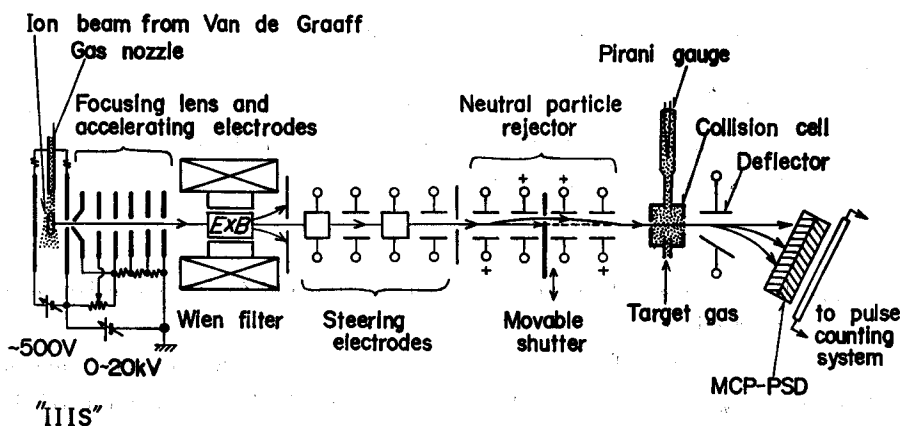
Fig. 1. Schematic diagram of the experimental arrangement.

The charge and energy of these ions were analyzed in a Wien filter ($E \times B$ field) and then the course was ajusted slightly by two pairs of steering electrodes. However, in order to prevent a heavy mixing of neutral components, it was necessary to arrange a "neutral particle rejector", which consisted of electrostatic deflectors and a movable shutter. Thus, a well resolved ion beam with the desired ionicity and energy could be introduced into a collision cell. The ion intensities were typically ~ 10 kcps for Ne^+, Ar^+, Kr^+ and Xe^+, but $10\sim100$ cps for Ne^{5+}, Ar^{7+}, Kr^{9+} and Xe^{11+}. Therefore, the time of data acquisition becomes longer as the projectile ionicity increases.

The collision cell was a SUS cylinder of 30 mmϕ $\times$ 40 mm$l$ with a 0.5 mmϕ entrance and 3.5 mmϕ exit apertures. Target gas was fed into this cell through a variable leak valve and the gas pressure was monitored with the use of a sensitive Pirani gauge, which had been calibrated by a capacitance manometer (Baratron). The main chamber was evacuated up to the base pressure of less than 2×10^{-7} Torr (2.7×10^{-5} Pa), the pumping system of which consisted of a 250 l/s turbomolecular pump and a 6" oil diffusion pump plus a liquid nitrogen trap,

2.2. System of particle detection

The charge-transferred outgoing ions were electrostatically deflected and hit on a position sensitive detector (PSD) separately according to their charges. This PSD was made of a rectangular (46mm $\times$ 13mm) tandem microchannel plate (MCP)*, onto which a resistive anode was attached. The output signals were processed in an analog decoder and also in a digital decoder, and so the position (charge) spectrum could be obtained with a good resolution. The details of the present MCP$-$PSD device have been reported elsewhere[6].

2.3. Determination of cross sections and uncertainties

The cross section values were derived by applying a growth rate method based

---

* Specially manufactured by Hamamatsu TV. Co., Ltd.

on the so-called rate equations. When ions of $q+$ ionicity pass through the collision cell, the peak corresponding to $(q-k)+$ ions ($k=0$, 1, 2, $\cdots$) appears on the PSD profile where k is the number of transferred electrons. If the fraction is denoted as $F_{q,q-k}$, it is a function of target thickness π (gas pressure $\times$ cell length), and we obtain its approximate expression in a low π region

$$F_{q,q-k}=\sigma_{q,q-k} \cdot \pi + C_k \cdot \pi^2,$$

where $\sigma_{q,q-k}$ is the cross section for k-electron transfer and C_k is a coefficient including several cross sections.

We measured a set of fraction curves for a given projectile-target combination and derived the $\sigma_{q,q-k}$ values by the least squares method. To examine the reliability of the above procedure, we solved the rate equations by using the $\sigma_{q,q-k}$ results. The reproductions were found satisfactory in most cases, and an example is shown in Fig. 2 for Ne^{4+} ions on He,

Each statistical deviation of $\sigma_{q,q-k}$ is easily obtained by the fitting procedure stated above, and typically a few % for $k=1$, 2 and 3. Other experimental uncertainties which affect the cross section values are listed in Table 2. The total experimental uncertainties for the absolute values of the cross section were obtained by the quadrature sum of these uncertainties. The reason for ion impurity is that our Wien filter is a $(q/m)^{1/2}$ analyzer and cannot separate ions with close q/m values. Therefore, contaminant $^{16}O^{4+}$ and $^{12}C^{3+}$ ions in $^{20}Ne^{5+}$, O^{2+} in Ar^{5+}, OH^+ and O^+ in Kr^{5+} and Xe^{8+}, N^+ in Kr^{6+} and Xe^{9+}, C^+ in Kr^{7+} and Xe^{11+}, and O_2^+ in Xe^{4+} were inevitably mixing. The amounts of these impurities were usually negligibly small or at most less than 5%. A large amount of contaminant C^+ ions, however, was found in Xe^{11+} ions and estimated to be about 39% in the case of $Xe^{11+}-$He collision, These contributions were corrected in deriving the final $\sigma_{q,q-k}$ values.
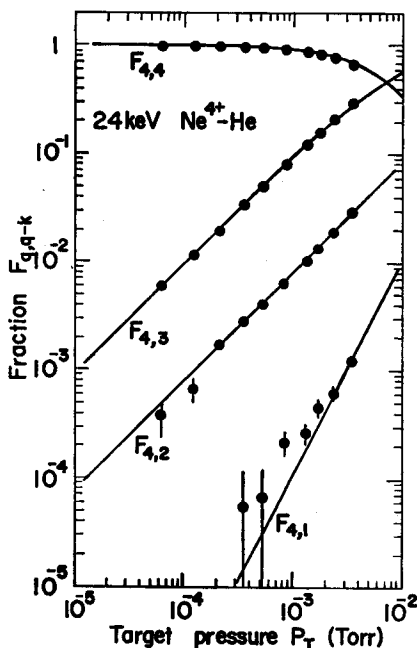

Fig. 2. Variations of charge fractions as a function of target gas pressure for 24 keV Ne^{4+} ions on He. Solid curves are the calculated fractions by using the experimental $\sigma_{q,q-k}$ values.

Table 2. List of systematic uncertainties.

Origin	Uncertainty (%)
Measurements of gas pressure	7
Effective collision length	5
Temperature	3
Target gas impurity	< 5
Ion impurity*	5 for $Kr^{5\sim7+}$ 4 for Ar^{5+} 3 for $Xe^{8,9+}$ 2 for Xe^{4+} < 1 for other ions except Xe^{11+}
Charge separation in PSD and error of dividing processor	<10 for Xe^{11+} < 5 for other ions

* The impurity contents in Xe^{11+} ions were estimated to be 8~40%, the contributions of which are corrected in deriving the cross section values.

3.   Results and comparison with other data

The present charge transfer cross sections are given in Tables 3 to 7 and are depicted in Figs. 3 to 15. The values obtained by other research workers are inserted in these figures for the sake of comparison.

3.1. $Ne^{q+}(q=2\sim5)$ ions on He

The energy range adopted is $1.5-12$ keV/q as listed in Table 3, and the present data together with those of others are plotted in Fig. 3. Our $\sigma_{2,1}$ results stay around

Table 3. Charge transfer cross sections for $Ne^{q+}(q=2\sim5)$ ions on He.

Ion^{q+}	Target	Energy (keV)	Cross section (cm²)	
			$\sigma_{q,q-1}$	$\sigma_{q,q-2}$
Ne^{2+}	He	3.0	$2.99\pm0.37(-17)$	$1.97\pm0.32(-18)$
		6.0	$5.01\pm0.66(-17)$	$4.65\pm0.85(-18)$
		12.0	$5.78\pm0.67(-17)$	$9.69\pm2.27(-18)$
		24.0	$8.50\pm1.00(-17)$	$1.17\pm0.16(-17)$
Ne^{3+}	He	5.3	$1.49\pm0.17(-16)$	$9.42\pm1.41(-18)$
		9.0	$1.28\pm0.15(-16)$	$8.22\pm1.22(-18)$
		18.0	$9.30\pm1.17(-17)$	$1.03\pm0.16(-17)$
		36.0	$1.11\pm0.15(-16)$	$1.06\pm0.20(-17)$
Ne^{4+}	He	6.0	$1.14\pm0.13(-15)$	$7.91\pm1.06(-17)$
		12.0	$9.60\pm1.13(-16)$	$7.21\pm0.86(-17)$
		24.0	$7.11\pm0.83(-16)$	$5.57\pm0.66(-17)$
		48.0	$7.27\pm0.85(-16)$	$3.78\pm0.49(-17)$
Ne^{5+}	He	15.0	$2.08\pm0.54(-15)$	——
		55.0	$1.69\pm0.40(-15)$	——

the mean of the values obtained by Flaks et al.[7], Cocke et al[8]. and Salzborn et al[9]., and can be connected with the higher energy data of Bloemen et al[10]. and Suk et al[11]. The present $\sigma_{2,0}$ results are rather consistent with those of Flaks et al[7]. Both $\sigma_{2,1}$ and $\sigma_{2,0}$ increase steeply with an increasing impact energy. This means that the electron transfer range, R_x, is rapidly increasing since $\sigma \propto \pi R_x^2$ is approximated,

The present values for Ne^{3+} to Ne^{5+} ions are rather monotone against ion energy, and are generally consistent with those of Cocke et al[8]. and Salzborn et al[9].

3.2.　$Kr^{q+}(q=4, 8)$ ions on He

The measurements were done in an energy range from 1.5 to 12 keV/q, as tabulated in Table 4 and represented in Fig. 4. The present data are original and are comparable with only the observations of Cocke et al[8]. at a lower impact energy. The cross section magnitudes are monotone against ion energy except for the present $\sigma_{4,3}$ values.

3.3.　$Ar^{q+}(q=2\sim7)$, $Kr^{q+}(q=2\sim9)$ and Xe^{q+} $(q=2\sim11)$ ions on He

The projectile q-dependence of the charge transfer cross section is quite important from the points of empirical scaling law and theoretical
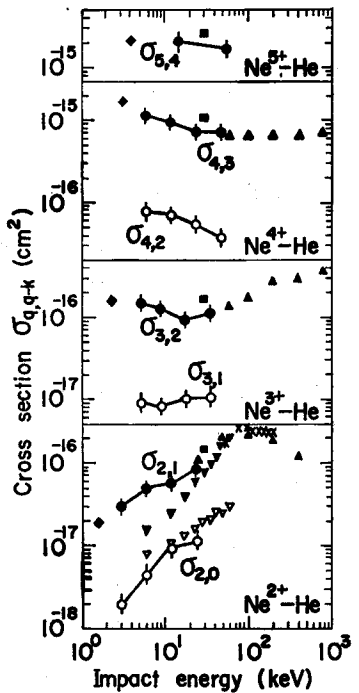
Fig. 3　Charge transfer cross sections for 1.5−12 keV/q Ne^{q+} ($q=$ 2~5) ions on He. Solid symbols and crosses denote single-electron transfer and open symbols stand for double-electron transfer.
●, ○: present-Kyoto, ▼, ▽: Flaks et al[7]., ◆: Cocke et al[8]., ■: Salzborn et al[9]., ▲: Bloemen et al[10]., ✕: Suk et al[11]. Solid lines are drawn to guide the eye.
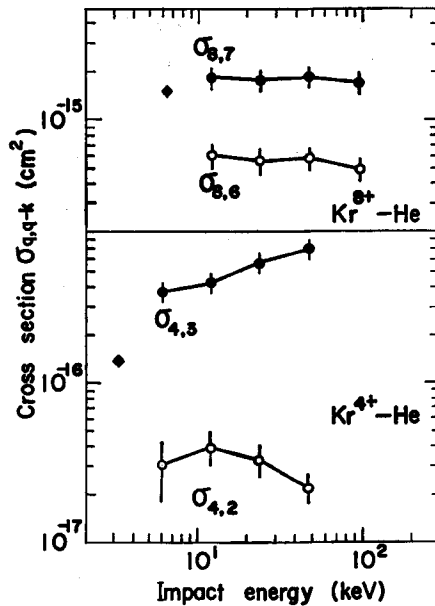
Fig. 4.　Charge transfer cross sections for 1.5−12 keV/q Kr^{q+} ($q=4$, 8) ions on He. Symbols are the same as in Fig. 3.

Table 4.　Charge transfer cross sections for Kr^{q+} ($q=4. 8$) ions on He.

Ion^{q+}	Target	Energy (keV)	Cross section (cm^2)	
			$\sigma_{q,q-1}$	$\sigma_{q,q-2}$
Kr^{4+}	He	6. 0	$3. 68\pm0. 45(-16)$	$3. 00\pm1. 26(-17)$
		12. 0	$4. 21\pm0. 52(-16)$	$3. 91\pm0. 94(-17)$
		24. 0	$5. 67\pm0. 70(-16)$	$3. 29\pm0. 73(-17)$
		48. 0	$6. 90\pm0. 81(-16)$	$2. 18\pm0. 39(-17)$
Kr^{8+}	He	12. 0	$1. 85\pm0. 22(-15)$	$6. 03\pm0. 76(-16)$
		24. 0	$1. 79\pm0. 22(-15)$	$5. 58\pm0. 98(-16)$
		48. 0	$1. 86\pm0. 22(-15)$	$5. 84\pm0. 78(-16)$
		96. 0	$1. 71\pm0. 21(-15)$	$4. 87\pm0. 67(-16)$

Table 5.　Charge transfer cross sections for Ar^{q+} ($q=2\sim7$), Kr^{q+} ($q=2\sim9$) and Xe^{q+} ($q=2\sim11$) ions on He at 0. 286 keV/amu in energy.

Ion	q	Target	Cross section (cm^2)	
			$\sigma_{q,q-1}$	$\sigma_{q,q-2}$
Ar^{q+}	2	He	$4. 72\pm0. 57(-16)$	$<0. 7(-18)$
	3		$4. 67\pm0. 56(-16)$	$5. 81\pm3. 24(-18)$
	4		$1. 02\pm0. 13(-15)$	$3. 41\pm1. 15(-17)$
	5		$1. 85\pm0. 23(-15)$	$2. 46\pm0. 33(-16)$
	6		$2. 28\pm0. 27(-15)$	$6. 59\pm0. 78(-16)$
	7		$2. 26\pm0. 29(-15)$	$5. 94\pm0. 70(-16)$
Kr^{q+}	2	He	$8. 25\pm0. 99(-17)$	$1. 71\pm0. 22(-18)$
	3		$1. 19\pm0. 15(-15)$	$3. 20\pm1. 15(-18)$
	4		$5. 67\pm0. 70(-16)$	$3. 29\pm0. 73(-17)$
	5		$1. 26\pm0. 17(-15)$	$9. 10\pm1. 15(-17)$
	6		$1. 54\pm0. 20(-15)$	$1. 68\pm0. 25(-16)$
	7		$2. 24\pm0. 31(-15)$	$7. 94\pm1. 14(-16)$
	8		$1. 79\pm0. 22(-15)$	$5. 58\pm0. 98(-16)$
	9		$2. 64\pm0. 33(-15)$	$1. 31\pm0. 50(-16)$
Xe^{q+}	2	He	$1. 79\pm0. 22(-17)$	$9. 52\pm1. 41(-18)$
	3		$4. 19\pm0. 49(-16)$	$1. 90\pm0. 47(-18)$
	4		$1. 57\pm0. 19(-15)$	$4. 66\pm1. 04(-18)$
	5		$1. 02\pm0. 13(-15)$	$1. 36\pm0. 42(-17)$
	6		$2. 22\pm0. 26(-15)$	$1. 30\pm0. 17(-16)$
	7		$2. 64\pm0. 31(-15)$	$5. 28\pm0. 75(-16)$
	8		$2. 38\pm0. 29(-15)$	$6. 30\pm0. 77(-16)$
	9		$3. 27\pm0. 41(-15)$	$2. 61\pm0. 51(-16)$
	10		$4. 00\pm0. 84(-15)$	$1. 55\pm0. 43(-16)$
	11		$5. 34\pm0. 99(-15)*$	$1. 56\pm0. 61(-16)*$

* These values are corrected for a 39% C^+ contamination mixing in Xe^{11+} ions.
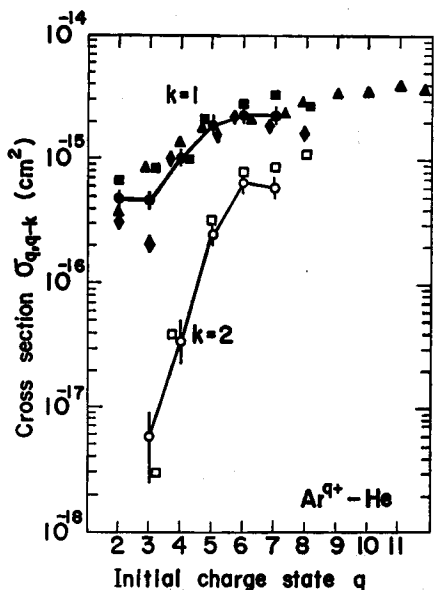
Fig. 5.   Charge transfer cross sections for 0. 286
keV/amu Ar^{q+} $(q=2\sim7)$ ions on He.
Solid and open symbols denote single-
and double-electron transfer, respecti-
vely.
●, ○: present-Kyoto, ■, □: Salzborn
et al[9,12]., ▲: Bliman et al[13]., ◆: Cocke
et al[14].
Solid lines are drawn to guide the eye.

Fig. 6.   Charge transfer cross sections for 0. 286
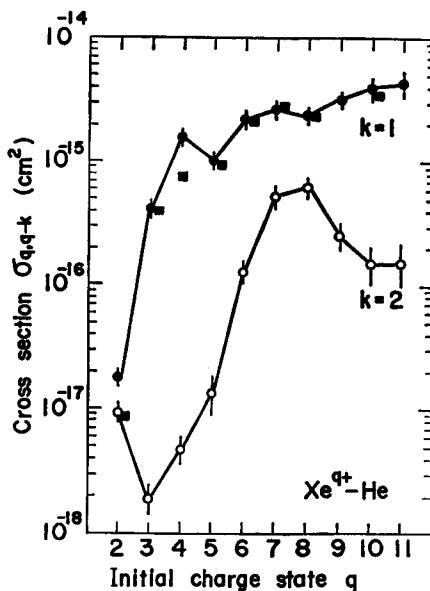keV/amu Kr^{q+} $(q=2\sim9)$ ions on He.
For symbols. see Fig. 5.

consideration.   The present results are
listed in Table 5 and are also illustrated
in Figs. 5, 6 and 7 for Ar^{q+}, Kr^{q+} and
Xe^{q+} ions, respectively.

Our $\sigma_{q,q-1}$ data for Ar^{q+} ions are in
general agreement with those of Salz-
born[9,12] (at 30 keV), Bliman[13] (mean
values in the energy range from $2q$ to
$10q$ keV) and Cocke[14] (at 0. 5 keV/q)
for $q\geq4$.   The scatter of these observa-
tions would be attributable to the ion-
energy dependence of the cross section.
The present $\sigma_{q,q-2}$ values are consistent
with those obtained by Salzborn et al[12].

Fig. 7.   Charge transfer cross sections for 0. 286
keV/amu Xe^{q+} $(q=2\sim11)$ ions on He.
For symbols, see Fig. 5.

In Fig. 6 are compared our $\sigma_{q,q-1}$ measurements and those of Cocke *et al*[14]. for Kr^{q+} ions, and an accordance is seen except for $q=4$. The deviation of $\sigma_{4,3}$ values also seems to be attributable to the energy dependence of the cross section. The $\sigma_{q,q-2}$ data have never been reported and we find a σ maximum at $q=7$ in the present study. Similarly, the results for Xe^{q+} ions are represented in Fig. 7, where the $\sigma_{q,q-1}$ values of Salzborn *et al*[9]. are compared. The $\sigma_{q,q-2}$ measurements in the $Xe^{q+}-He$ collision had been firstly done by our study group.

3.4. $Kr^{q+}(q=2\sim9)$ ions on Ne, Ar, Kr and Xe

It is very interesting to survey the charge transfer collisions of multiply vacant ions with multi-electron targets at a given energy. The $\sigma_{q,q-k}$ data for Kr^{q+} ions on Ne, Ar, Kr and Xe are compiled in Table 6 and graphically shown in Figs. 8, 9, 10 and 11, respectively.

The comparable observations are quite poor, and there have been reported only the $\sigma_{q,q-1}$ data of Salzborn *et al*[9]. for the $Kr^{q+}-Ar$ case at 30 keV, which are consistent with ours. The feature is that the $\sigma_{q,q-k}$ values have a similar trend against q as
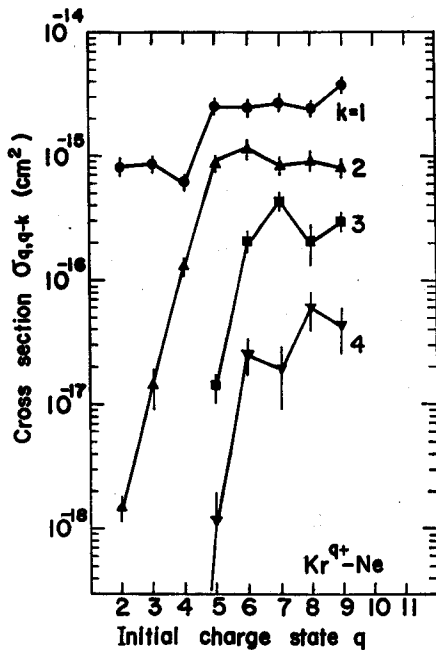
Fig. 8. Charge transfer cross sections for 0.286 keV/amu $Kr^{q+}(q=2\sim9)$ ions on Ne. ●, ▲, ■, ▼: present-Kyoto. The notation k means the number of transferred electrons. Solid lines are served to guide the eye.
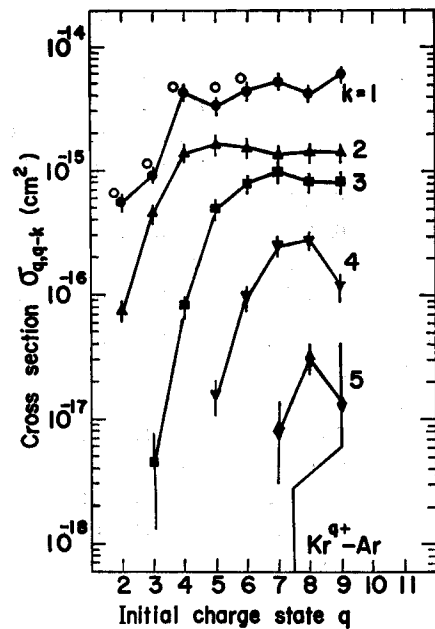
Fig. 9. Charge transfer cross sections for 0.286 keV/amu $Kr^{q+}(q=2\sim9)$ ions on Ar. ●, ▲, ■, ▼, ◆: present-Kyoto, ○: Salzborn *et al*[9]. Other notations are the same as in Fig. 8.
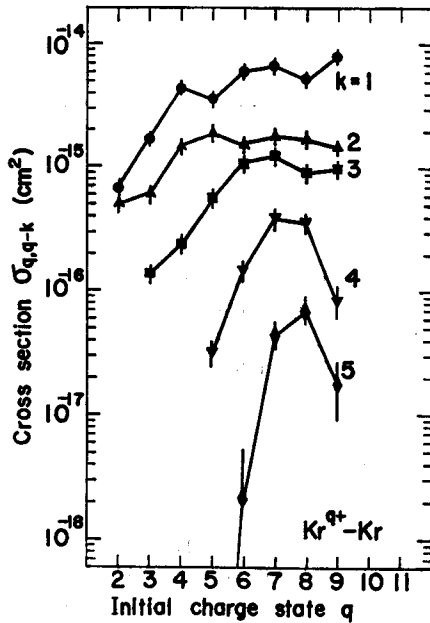
Fig. 10. Charge transfer cross sections for 0.286 keV/amu Kr^{q+} ($q=2\sim9$) ions on Kr. Symbols and notations are the same as in Fig. 9.
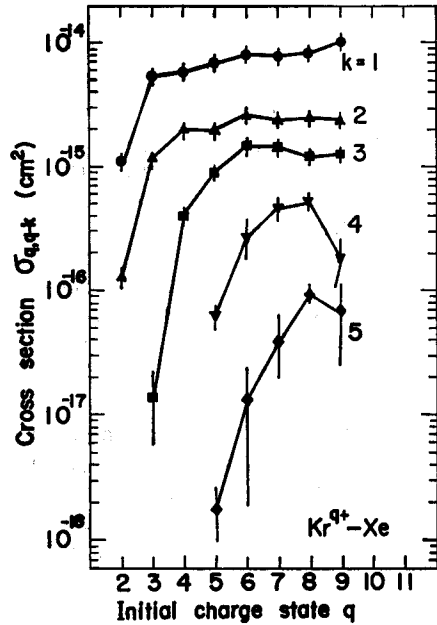
Fig. 11. Charge transfer cross sections for 0.286 keV/amu Kr^{q+} ($q=2\sim9$) ions on Xe. Symbols and notations are the same as in Fig. 9.

are listed in Table 7 and are depicted in Figs. 12, 13, 14 and 15 for Ne, Ar. Kr and Xe, respectively. The Salzborn data[9] obtained at 30 keV are inserted, which show a systematic overestimation from our results. Again, there are seen remarkable behaviors whereby the $\sigma_{q,q-k}$ results have a similar trend against q and k, but no significant σ maxima are seen.

4. Summary

We have measured the cross sections of single- to multiple-electron transfer for slow multiply ionized Ne, Ar, Kr and Xe ions on rare gas targets, and the results are compiled here. The features are summarized as follows:

(1) The cross sections for single-electron transfer, $\sigma_{q,q-1}$, have oscillations against q. This fact is consistent with the prediction of a "classical one electron model" (COEM)[15].

(2) The σ data of Salzborn's group[9,12] are in general accordance with the present results, but deviate for targets with small ionization potentials. Therefore, the reported scaling law[9] for $\sigma_{q,q-1}$ should be reexamined.

(3) The double-electron transfer cross sections, $\sigma_{q,q-2}$, for Ar^{q+}, Kr^{q+} and Xe^{q+}

46   Toshio KUSAKABE, Hirofumi HANAKI, Nobuo NAGAI, Tadahiko HORIUCHI, Ichiro KONOMI
and Masakatsu SAKISAKA

Table 7. Charge transfer cross sections for Xe^{q+} ($q=2\sim11$) ions on Ne, Ar, Kr and
Xe at 0.286 keV/amu in energy.

Ion q Target	Cross section (cm²)				
	$\sigma_{q,q-1}$	$\sigma_{q,q-2}$	$\sigma_{q,q-3}$	$\sigma_{q,q-4}$	$\sigma_{q,q-5}$
Xe^{q+} 2⁺ Ne	9.19±1.17(−17)	<3.5(−18)	——	——	——
3	1.82±0.29(−15)	<3.0(−18)	——	——	——
4	1.08±0.14(−15)	8.16±4.51(−17)	<1.0(−17)	——	——
5	1.61±0.19(−15)	1.55±0.32(−16)	2.22±1.31(−17)	——	——
6	2.87±0.34(−15)	9.92±1.26(−16)	3.59±1.35(−17)	——	——
7	2.56±0.56(−15)	1.16±0.26(−15)	9.85±3.22(−17)	1.68±3.61(−17)	——
8	2.20±0.28(−15)	8.98±1.10(−16)	3.24±0.43(−16)	1.97±1.05(−17)	——
9	3.59±0.46(−15)	1.05±0.16(−15)	1.30±0.48(−16)	1.90±1.08(−17)	——
10	4.17±0.49(−15)	9.97±1.24(−16)	2.19±0.33(−16)	4.18±1.66(−17)	——
11	——	——	——	——	——
Xe^{q+} 2⁺ Ar	1.88±0.22(−15)	1.92±0.37(−17)	——	——	——
3	8.04±0.94(−16)	4.09±0.49(−16)	3.31±0.47(−17)	——	——
4	3.46±0.42(−15)	1.32±0.16(−15)	3.71±1.22(−17)	——	——
5	3.84±0.45(−15)	1.73±0.20(−15)	2.70±0.34(−16)	——	——
6	2.95±0.52(−15)	1.74±0.22(−15)	6.37±0.81(−16)	5.01±1.36(−17)	——
7	5.41±0.63(−15)	1.57±0.19(−15)	8.02±1.01(−16)	1.15±0.20(−16)	2.15±1.98(−17)
8	4.78±0.58(−15)	1.65±0.21(−15)	9.33±1.19(−16)	1.64±0.38(−16)	3.02±0.76(−17)
9	6.57±0.80(−15)	1.50±0.18(−15)	8.73±1.08(−16)	1.50±0.19(−16)	1.92±0.81(−17)
10	7.13±0.84(−15)	1.74±0.21(−15)	7.76±0.91(−16)	1.46±0.43(−16)	3.98±1.41(−17)
11	7.67±1.86(−15)*	1.63±0.40(−15)*	8.45±2.25(−16)*	1.47±0.83(−16)*	7.13±3.57(−17)*
Xe^{q+} 2⁺ Kr	9.82±1.14(−16)	9.23±1.30(−17)	——	——	——
3	9.76±1.23(−16)	8.29±1.09(−16)	3.58±0.49(−17)	——	——
4	5.04±0.60(−15)	1.80±0.21(−15)	1.15±0.15(−16)	——	——
5	4.40±0.52(−15)	2.13±0.26(−15)	4.69±0.55(−16)	——	——
6	5.05±0.59(−15)	2.20±0.26(−15)	8.40±1.01(−16)	6.71±0.92(−17)	1.10±0.42(−17)
7	5.90±0.70(−15)	1.88±0.22(−15)	1.15±0.14(−15)	1.75±0.28(−16)	1.93±0.50(−17)
8	5.61±0.68(−15)	1.78±0.22(−15)	1.05±0.13(−15)	2.56±0.35(−16)	1.62±0.71(−17)
9	8.19±1.00(−15)	1.87±0.23(−15)	1.12±0.14(−15)	2.06±0.26(−16)	2.70±1.22(−17)
10	9.83±1.15(−15)	1.95±0.24(−15)	1.08±0.14(−15)	1.93±0.26(−16)	4.15±1.72(−17)
11	1.01±0.19(−14)*	2.29±0.43(−15)*	1.29±2.27(−15)*	2.36±0.52(−16)*	5.53±3.54(−17)*
Xe^{q+} 2 Xe	8.71±1.20(−16)	6.74±1.03(−16)	——	——	——
3	3.54±0.41(−15)	9.91±1.15(−16)	1.45±0.18(−16)	——	——
4	5.94±0.70(−15)	2.12±0.25(−15)	2.73±0.53(−16)	2.55±0.98(−17)	——
5	4.14±0.49(−15)	2.82±0.33(−15)	7.49±0.95(−16)	3.07±0.76(−17)	2.13±0.51(1.17)
6	7.02±0.82(−15)	2.17±0.25(−15)	1.29±0.15(−15)	1.16±0.23(−16)	7.19±3.17(−17)
7	7.01±0.83(−15)	2.34±0.28(−15)	1.41±0.17(−15)	3.73±0.44(−16)	2.55±0.42(−17)
8	6.63±0.80(−15)	2.29±0.28(−15)	1.26±0.16(−15)	3.78±0.59(−16)	3.38±1.48(−17)
9	1.08±0.14(−14)	2.27±0.28(−15)	1.46±0.27(−15)	3.06±0.41(−16)	6.07±2.26(−17)
10	1.19±0.14(−14)	2.87±0.35(−15)	1.34±0.16(−15)	4.75±0.80(−16)	1.55±0.32(−16)
11	——	——	——	——	——

⁺ Only these collisions were measured at 0.262 keV/amu in energy to prevent an eletrical
breakdown in ion acceleration,

* These values are corrected by considering the 28.8 and 20.4% C^+ contaminations in Xe^{11+}
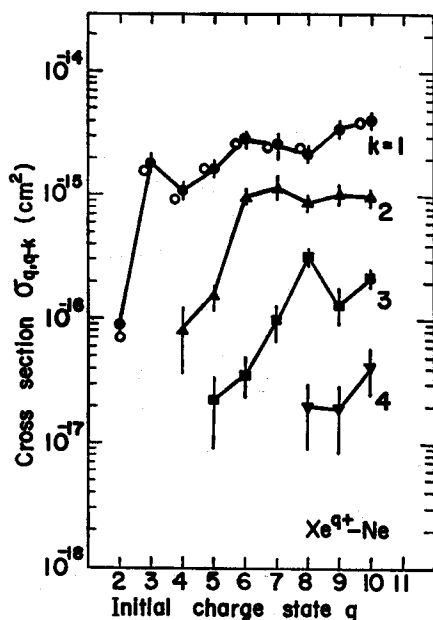ions on Ar and Kr, respectively,

Fig. 12. Charge transfer cross sections for 0.286 keV/amu Xe^{q+} ($q=2\sim11$) ions on Ne. Symbols and notations are the same as in Fig. 9.
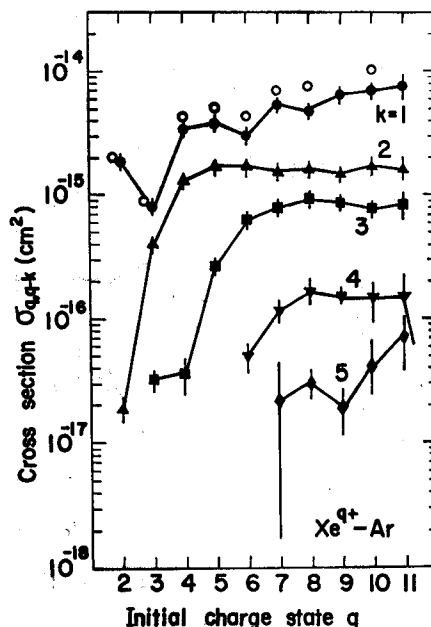
Fig. 13. Charge transfer cross sections for 0.286 keV/amu Xe^{q+} ($q=2\sim11$) ions on Ar. Symbols and notations are the same as in Fig. 9.

on He show a very similar dependence on q and have clear maxima at around $q=7$.

(4) The multiple-electron transfer cross sections for Kr^{q+} and Xe^{q+} ions on Ar, Kr and Xe behave very similarly irrespective of target gas. A comparison with the "classical absorbing sphere model" (CASM)[16] could be done, but at present, it is only a measure to know the $\sigma_{q,q-k}$ behaviors and magnitudes. A new treatment of the "statistical electron transfer model" (SETM)[17] proposed by our study group seems useful.

(5) The compiled data include many important facts to be profoundly examined, which are to be discussed elsewhere.

Ackowledgements

48 Toshio KUSAKABE, Hirofumi HANAKI, Nobuo NAGAI, Tadahiko HORIUCHI, Ichiro KONOMI
and Masakatsu SAKISAKA
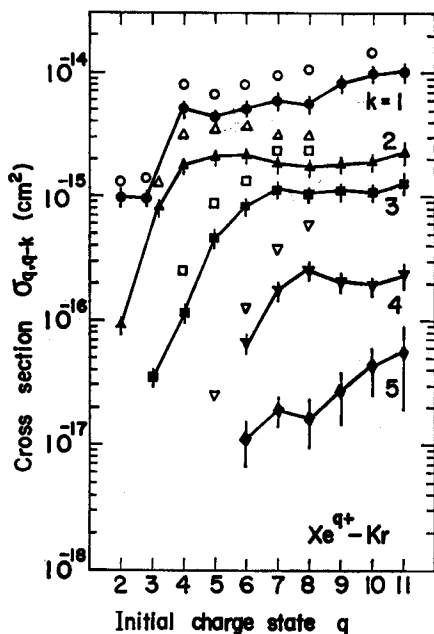
Fig. 14. Charge transfer cross sections for 0.286 keV/amu Xe^{q+} ($q=2\sim11$) ions on Kr. ●, ▲, ■, ▼, ◆: present-Kyoto, ○, △, □, ▽, : Salzborn et al[9]. Other notations are the same as in Fig. 9.
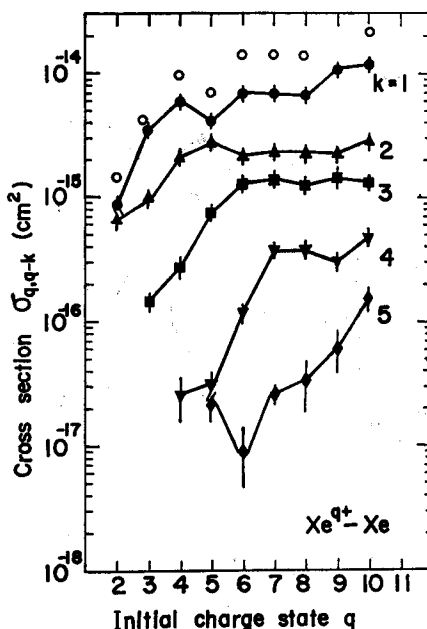
Fig 15. Charge transfer cross sections for 0.286 keV/amu Xe^{q+} ($q=2\sim11$) ions on Xe. Symbols and notations are the same as in Fig. 9.

References

1) A. Dalgarno and S. E. Butler; Comm. Atom. Mol. Phys., 7, 129 (1978).

2) Proc. Nagoya Semi. on Atomic Processes in Fusion Plasmas, Nagoya, IPPJ-AM-13, (1978).

3) T. Kusakabe, H. Hanaki, N. Nagai, K. Kuroda, N Maeda and M. Sakisaka; Nucl. Instr. Meth., 198, 577 (1982).

4) T. Kusakabe, H. Hanaki, N. Nagai, T. Horiuchi and M. Sakisaka; Physica Scripta, T3, 191 (1983).

5) H. Hanaki, T. Kusakabe, N. Nagai and M. Sakisaka; J. Phys. Soc. Japan, 52, 424 (1983).

6) H. Hanaki, N. Nagai, T. Kusakabe, T. Horiuchi and M. Sakisaka; Japan. J. Appl. Phys., 22, 201 (1983).

7) I. P. Flaks and E. S. Solov'ev; Sov. Phys. Tech. Phys., 3, 577 (1958).

8) C. L. Cocke, R. Dubois, T. J. Gray and E. Justiniano; IEEE Trans. Nucl. Sci., NS-28, 1032 (1981).

9) E. Salzborn and A. Müller; Electronic and Atomic Collisions, Invited papers of the XI-ICPEAC, Kyoto, (North Holland, Amsterdam), p. 407 (1979).

10) E. W. P. Bloemen, D. Dijkkamp and F. J. de Heer; J. Phys. B, 15, 1391 (1981).

11) H. C. Suk, A. Guilbaud and B. Hird; J. Phys. B, 11, 1463 (1978).

12) A. Müller and E. Salzborn; Phys. Lett., 59A, 19 (1976).

13) S. Bliman, J. Aubert, R. Geller, B. Jacquot and D. Van. Houtte; Phys. Rev., A23, 1703 (1981).

14) C. L. Cocke, R. Dubois, T. J. Gray, E. Justiniano and C. Can; Phys. Rev. Lett., 46, 1671

(1981).

15) H. Ryufuku, K. Sasaki and T. Watanabe; Phys. Rev., **A21**, 745 (1980).

16) R. K. Janev and L. P. Presnyakov; Physics Reports, **70**, 82 (1981).

17) M. Sakisaka, H. Hanaki, N. Nagai, T. Horiuchi, I. Konomi and T. Kusakabe; J. Phys. Soc. Japan, **52**, 716 (1983).